



The nature of π -hole interactions between iodide anions and quinoid rings in the crystalline state

Valentina Milašinović, Vedran Vuković, Anna Krawczuk, Krešimir Molčanov, Christoph Hennig and Michael Bodensteiner

IUCrJ (2023). **10**, 156–163



IUCr Journals

CRYSTALLOGRAPHY JOURNALS ONLINE

This open-access article is distributed under the terms of the Creative Commons Attribution Licence <https://creativecommons.org/licenses/by/4.0/legalcode>, which permits unrestricted use, distribution, and reproduction in any medium, provided the original authors and source are cited.



The nature of π -hole interactions between iodide anions and quinoid rings in the crystalline stateValentina Milašinović,^a Vedran Vuković,^b Anna Krawczuk,^c Krešimir Molčanov,^{a*} Christoph Hennig^{d,e} and Michael Bodensteiner^b^aDepartment of Physical Chemistry, Rudjer Bošković Institute, Bijenička 54, Zagreb 10000, Croatia, ^bUniversität Regensburg, Universitätsstrasse 31, 93053 Regensburg, Germany, ^cInstitut für Anorganische Chemie, Universität Göttingen, Tammannstraße 4, 37077 Göttingen, Germany, ^dThe Rossendorf Beamline (BM20), European Synchrotron Radiation Facility, 71 Avenue des Martyrs, Grenoble 38043, France, and ^eInstitute of Resource Ecology, Helmholtz Zentrum Dresden Rosendorf, Bautzner Landstrasse 400, 01328 Dresden, Germany. *Correspondence e-mail: kmolcano@irb.hrReceived 16 May 2022
Accepted 3 January 2023

Edited by M. Eddaoudi, King Abdullah University, Saudi Arabia

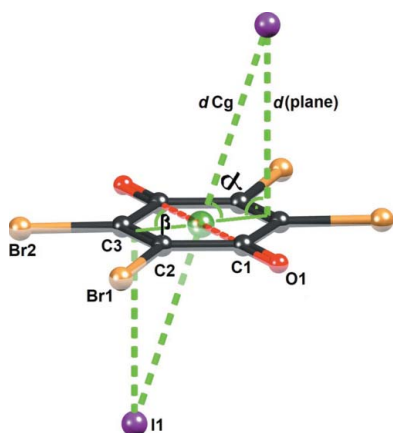
Keywords: π -hole interactions; charge transfer; quinone; charge density; Atoms In Molecule analysis.**CCDC reference:** 2234264**Supporting information:** this article has supporting information at www.iucrj.org

The investigated co-crystal of 3-chloro-*N*-methylpyridinium iodide with tetrabromoquinone (3-Cl-*N*-MePy·I·Br₄Q) reveals a π -hole interaction between an iodide anion and a quinoid ring involving an $n \rightarrow \pi^*$ charge transfer. The quinoid ring has a partial negative charge (estimated to be in the range 0.08–0.11 e) and a partial radical character, which is related to the black colour of the crystals (crystals of neutral tetrabromoquinone are yellow). A detailed X-ray charge density study revealed two symmetry-independent bond critical points between the iodide anions and carbon atoms of the ring. Their maximum electron density of 0.065 e Å⁻³ was reproduced by quantum chemical modelling. The energy of the interaction is estimated to be -11.16 kcal mol⁻¹, which is comparable to the strength of moderate hydrogen bonding (about -10 kcal mol⁻¹); it is dominantly electrostatic in nature, with a considerable dispersion component.

1. Introduction

π -hole interactions, *i.e.* interactions involving areas of electron depletion in π -electron systems, have attracted considerable attention in the fields of supramolecular chemistry and crystal engineering (Frontera *et al.*, 2011; Wang & Wang, 2013; Kozuch, 2016; Angarov & Kozuch, 2018; Grounds *et al.*, 2018; Jia *et al.*, 2019; Kumar Seth *et al.*, 2019). An electrostatic interaction occurs between the π -hole and an electron-rich group involving a lone electron pair [lone pair- π or lp $\cdots\pi$ interaction (Mooibroek *et al.*, 2008; Singh & Das, 2015; Newberry & Raines, 2017; Kumar Seth *et al.*, 2018; Angarov & Kozuch, 2018)] or an anion [anion- π interaction (Gamez *et al.*, 2007; Schottel *et al.*, 2008; Frontera *et al.*, 2011; Wang & Wang, 2013; Bauzá *et al.*, 2016; Lucas *et al.*, 2016; Savastano *et al.*, 2017)]. The interaction may also involve charge transfer, typically from a lone pair to an antibonding orbital of the π system [$n \rightarrow \pi^*$ interaction (Mooibroek *et al.*, 2008; Singh & Das, 2015; Newberry & Raines, 2017; Angarov & Kozuch, 2018)]. They are interesting due to their potential application in molecular recognition (Wang & Wang, 2013; Lucas *et al.*, 2016; Zeng *et al.*, 2019) and drug design (Singh & Das, 2015), and have also been used in crystal engineering (Bauzá *et al.*, 2016; Kumar Seth *et al.*, 2019; Bauza *et al.*, 2019).

Even though the majority of studies have been carried out on electron-poor aromatic systems, quinoid rings, having electron-depleted carbonyl groups, are more promising acceptors of π -hole interactions (Molčanov *et al.*, 2018; Kepler *et al.*, 2019; Wilson *et al.*, 2020; Milašinović & Molčanov, 2021).



Quinones with four electronegative substituents have especially prominent π -holes (Molčanov *et al.*, 2019; Vuković *et al.*, 2019) and their interactions with halide anions often involve a charge transfer, indicated by a colour change of the compound (Molčanov *et al.*, 2018; Milašinić & Molčanov, 2021). The common structure motif of the compound under investigation is a sandwich-like group involving two close contacts between a quinone and two halide anions, $X^- \cdots Q \cdots X^-$ (Fig. 1). The interaction, involving charge transfer is presumably of $n \rightarrow \pi^*$ type, and is often related to the reduction of quinones to semiquinone radicals. It may be assumed that the 'sandwich' is an intermediate in the reduction of a quinone. Owing to its common formation it may be used in crystal engineering.

However, the nature and strength of this quinone–iodide interaction remains elusive, and a detailed study is difficult. The dark colour and opacity of the crystals impede studies that use optical spectroscopy, and the presence of heavy atoms (iodine and bromine) makes quantum chemical study challenging. The strong absorption limits the applicability of X-ray diffraction studies. Our initial work (Molčanov *et al.*, 2018) on a series of similar compounds used structural characterization that coupled infrared and solid-state NMR spectroscopies and quantum chemical computation [MP2 and periodic density functional theory (DFT)]. The results highlighted the $n \rightarrow \pi^*$ charge transfer and estimated the interaction energy to be 6–10 kcal mol⁻¹ (by the MP2 method). However, the degree of charge transfer remained an open issue. Most likely it is quite low (a few percent of an electron), which would be sufficient for a colour change, but not enough to be quantified by spectroscopic methods. A simple analysis of crystal structures using Hirshfeld surfaces (HSs), highest occupied molecular orbitals (HOMOs) and lowest unoccupied molecular orbitals (LUMOs) computed using the *CrystalExplorer* software (Spackman *et al.*, 2021) and analysis of Voronoi–

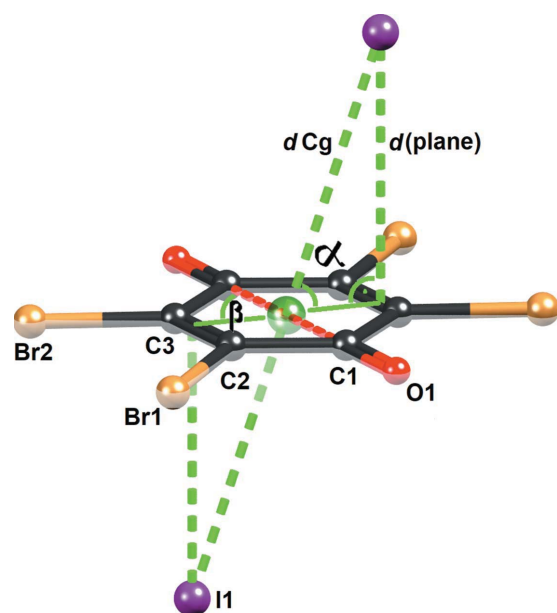


Figure 1
Sandwich-like $I^- \cdots Br_4Q \cdots I^-$ unit in **1** with geometric parameters indicated. Symmetry-independent atoms are labelled.

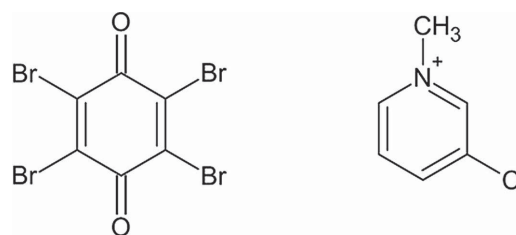


Figure 2
Tetrabromoquinone and 3-Cl-*N*-MePy cation.

Dirichlet polyhedra (VDP) (Blatov, 2004) confirmed this model (Milašinić & Molčanov, 2021).

In this work, we opted for a combined experimental and theoretical charge density study on a model system, a co-crystal of 3-chloro-*N*-methylpyridinium iodide and tetrabromoquinone [(3-Cl-*N*-MePy)₂I₂·Br₄Q, named **1**, Fig. 2]. To avoid absorption problems, we used short-wavelength (0.6 Å) high-intensity synchrotron radiation for the X-ray diffraction studies. The analysis of the electron density obtained is further supported by extensive theoretical calculations both in the gas phase and as a crystalline structure. This approach allows us to study in detail the behaviour of molecular orbitals in the areas of crucial interactions, interaction energies as well as provide discussion on the topological analysis of charge density.

2. Results and discussion

2.1. Crystal packing of **1**

The asymmetric unit of **1** comprises a 3-Cl-*N*-MePy cation, an iodide anion and half of a centrosymmetric Br₄Q molecule; therefore, the molecular formula is (3-Cl-*N*-MePy)₂I₂·Br₄Q. The easily recognized motif is a sandwich-like $I^- \cdots Br_4Q \cdots I^-$ unit (Fig. 1) which we have identified in similar compounds (Molčanov *et al.*, 2018; Milašinić & Molčanov, 2021). The distance from the iodide to the centroid of the quinoid ring is 3.947 Å, the distance to the ring mean plane is 3.727 Å and the angle α between the iodide–centroid axis and the ring plane is 72.0°. The iodide is offset by 1.220 Å approximately towards C2; the angle β defining the direction of the offset relative to the carbonyl–carbonyl axis is 76.8°. The only contact shorter than the sum of van der Waals radii for I and C (3.76 Å) is I1...C3 [3.7450 (7) Å].

Crystal packing can be described as cations inserted between $I^- \cdots Br_4Q \cdots I^-$ units (Fig. 3). Aside from the π -hole contact with Br₄Q, the iodide forms three halogen bonds, two with bromine from the Br₄Q molecules and one with a Cl from the cation (Table 1). It also forms two close contacts (3.70 Å) with N1 and C8 atoms from the cation, which are the result of electrostatic attraction between the cation and anion.

The quinone acts as electron donor of two symmetry-independent halogen bonds (a total of four; Table 1) and its oxygen atom accepts two weak hydrogen bonds from the cation (Table 2). A pair of inversion-related cations form a π -stacked pair with antiparallel C–Cl bonds (Fig. S9). The interplanar separation (the ring planes are parallel, so $\alpha = 0^\circ$) is 3.3879 (3) Å, but the rings are offset by 3.609 Å, so the

Table 1

Short halogen–halogen distances.

	d (Å)	C–Br⋯I (°)	Symmetry operations on Br
C2–Br1⋯I1	3.4960 (1)	173.54 (2)	$1 - x, -1/2 + y, 1/2 - z$
C3–Br2⋯I2	3.5781 (1)	172.29 (2)	$x, -1 + y, z$
C5–Cl1⋯I1	3.6225 (2)	168.89 (3)	$1 - x, 1 - y, 1 - z$
C5–Cl1⋯Cl1†	4.2631 (4)	87.76 (5)	$1 - x, 1 - y, 1 - z$

† Type II contact.

Table 2

Geometric parameters of hydrogen bonds.

	$D-H$ (Å)	$H\cdots A$ (Å)	$D\cdots A$ (Å)	$D-H\cdots A$ (°)	Symmetry operations on A
C4–H4⋯O1	1.08	2.11	3.1436 (13)	158	$1 + x, y, z$
C6–H6⋯Cl1†	1.08	2.78	3.8442 (8)	166	$-x, 1 - y, 1 - z$
C7–H7⋯I1	1.08	3.03	3.8402 (9)	132	$-1 + x, y, z$
C9A–H9A⋯O1†	1.08 (15)	2.41 (18)	3.4109 (14)	154 (7)	$1 + x, y, z$
C9–H9C⋯Br2†	1.1 (2)	2.8 (2)	3.8516 (9)	157 (6)	$1 - x, -1/2 + y, 1/2 - z$
C9–H9A⋯Br1‡	1.08 (15)	3.09 (4)	3.915 (10)	142 (11)	$1 + x, y, z$
C9–H9B⋯Br1‡	1.08 (11)	3.24 (10)	4.001 (10)	122 (2)	$1 - x, -1/2 + y, 1/2 - z$
C8–H8⋯Br1‡	1.08	3.21	4.168 (10)	147	$1 - x, -1/2 + y, 1/2 - z$

† Those found by geometric criteria, but lacking (3, -1) critical points. ‡ Those with (3, -1) critical points but unfavourable geometry.

centroid distance is rather large, 4.9503 (4) Å. This multitude of intermolecular interactions can be ranked according to their strength and importance as (i) cation–anion electrostatic interactions, (ii) iodide–quinone π -hole interactions, (iii) halogen bonding and (iv) stacking interactions between cations.

The importance of contacts with the iodide anion is illustrated by the HS of the Br₄Q molecule (Fig. 4): C⋯I contacts comprise 7.4% of the surface, whereas Br⋯I contacts

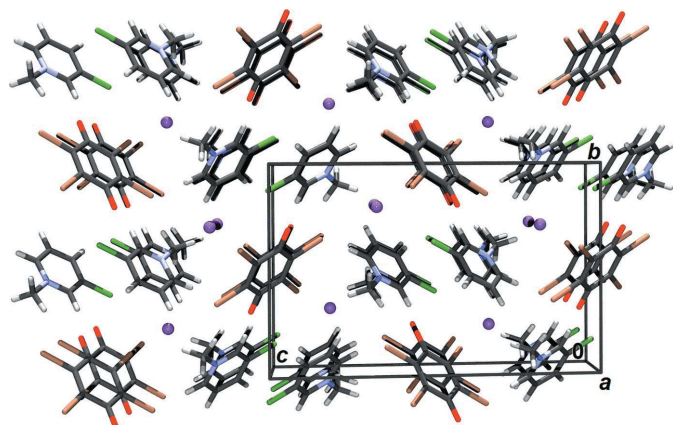


Figure 3

Crystal packing viewed approximately in the $\langle 100 \rangle$ direction. Iodide anions are shown as spheres of arbitrary radii.

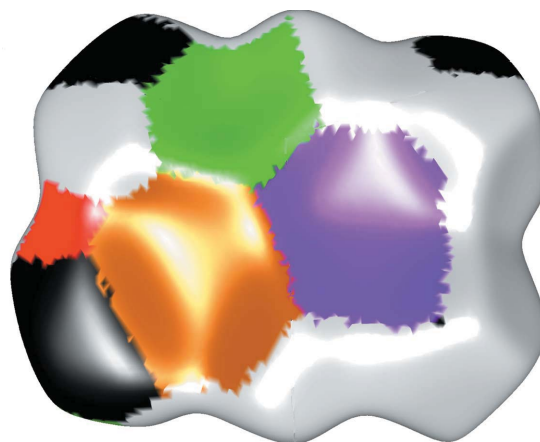


Figure 4

Hirshfeld surface of a Br₄Q molecule with closest-neighbour atoms colour coded: H – grey, C – black, O – red, Cl – green, Br – brown and I – purple.

(representing halogen bonding) comprise a further 7.3%. This is slightly higher than in a previously studied series of co-crystals [where the C⋯I contacts comprised 6–7% of the HS (Milašinić & Molčanov, 2021)]. The non-localized nature of the iodide–quinone interaction is also noted when the surface of a Br₄Q molecule is constructed using VDP (Blatov, 2004): 12 individual faces corresponding to 12 individual C⋯I contacts (six for each symmetry-independent C⋯I interaction, Fig. S10) have a total area of 16.64 Å² or 3.5% of the VDP surface. These contact areas are similar to those found in another series of compounds [typically 6–7% of the HS and 3–3.8% of the VDP surface (Milašinić & Molčanov, 2021)].

2.2. Analysis of intermolecular electron density and iodide–quinone contacts

Intermolecular critical points (Fig. 5, Table 3) are mostly in agreement with the geometric analysis of crystal packing. There are two (3, -1) critical points between the iodide and the quinoid ring, with respective electron densities of 0.040 and 0.014 e Å⁻³ (Table 3); the stronger one corresponds to a bond path between I1 and the most electron-depleted atom of the quinone C1 (Fig. 5). The same critical points have also been reproduced by a periodic DFT model, with somewhat higher electron densities of 0.065 and 0.042 e Å⁻³, respectively (Table 3). This is consistent with the electrostatic nature of the iodide–quinone interaction, thus the covalent component is likely negligible (see below).

The analysis of theoretical charges (Table 4) indicates a partial charge transfer from the iodide to the quinoid ring of -0.077 to -0.109e, implying a partial negative charge of the Br₄Q. This corresponds with the black colour of the crystals and confirms our previous conclusion (Molčanov *et al.*, 2018). It also provides a more reliable estimate of the degree of charge transfer, as our previous tentative computations were severely overestimated (Molčanov *et al.*, 2018). Therefore, the interaction is of the $n \rightarrow \pi^*$ type donates electrons into an empty π^* (*i.e.* LUMO) orbital of the quinone, which manifests

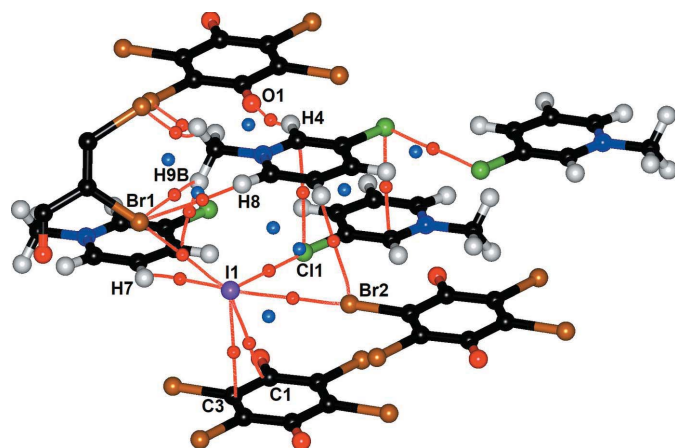
Table 3

 Experimental and calculated (italic) intermolecular bonding critical points in the crystal structure of **1**.

$A \cdots B$	d (Å)	Electron density ($\text{e}\text{Å}^{-3}$) ρ_{cp}	Laplacian ($\text{e}\text{Å}^{-5}$)	Type	Symmetry operation on B
π -hole					
I1 \cdots C1	4.1060 (7)	0.0141 <i>0.0424</i>	0.15 <i>0.40</i>	(3, -1)	$1 + x, -1 + y, z$
I1 \cdots C3	3.7450 (7)	0.0405 <i>0.0655</i>	0.42 <i>0.67</i>	(3, -1)	$1 + x, -1 + y, z$
Halogen bonding					
I1 \cdots Cl1	3.6225 (2)	0.0600 <i>0.0594</i>	0.61 <i>0.72</i>	(3, -1)	$1 - x, 1 - y, 1 - z$
Cl1 \cdots Cl1	4.2631 (4)	0.0112 <i>NO BCP FOUND</i>	0.15	(3, -1)	$1 - x, 1 - y, 1 - z$
I1 \cdots Br1	3.4960 (1)	0.0743 <i>0.0971</i>	0.73 <i>0.90</i>	(3, -1)	$1 - x, -1/2 + y, 1/2 - z$
I1 \cdots Br2	3.5781 (1)	0.0637 <i>0.0813</i>	0.62 <i>0.78</i>	(3, -1)	$x, -1 + y, z$
Hydrogen bonding					
H4 \cdots O1	2.11	0.0693 <i>0.1161</i>	1.79 <i>1.69</i>	(3, -1)	$1 + x, y, z$
H9A \cdots Br1	3.09 (4)	0.0228 <i>0.0378</i>	0.35 <i>0.48</i>	(3, -1)	$1 + x, y, z$
H8 \cdots Br1	3.21	0.0261 <i>0.0290</i>	0.32 <i>0.24</i>	(3, -1)	$1 - x, -1/2 + y, 1/2 - z$
H9B \cdots Br1	3.24 (10)	0.0341 <i>0.0321</i>	0.39 <i>0.34</i>	(3, -1)	$1 - x, -1/2 + y, 1/2 - z$
H9C \cdots Br2	2.8 (2)	0.0290 <i>0.0607</i>	0.47 <i>0.72</i>	(3, -1)	$1 - x, -1/2 + y, 1/2 - z$
H7 \cdots I1	3.8402 (9)	0.0559 <i>NO BCP FOUND</i>	0.49	(3, -1)	$-1 + x, y, z$
C–H \cdots π					
H9B \cdots C6	2.88 (5)	0.0457 <i>0.0320</i>	0.46 <i>0.36</i>	(3, -1)	$1 + x, y, z$
π -stacking					
Cl1 \cdots C4	3.4361 (7)	0.0452	0.54	(3, -1)	$1 - x, 1 - y, 1 - z$

in an overlap of LUMOs in Fig. 6. Similar behaviour can be observed in the highest binding orbital HOMO-6, where a slight overlap between the iodine orbitals and the quinone ring supports our suggestion that a non-covalent interaction of the π -hole type is present.

The total binding energy calculated for an $\text{I}^- \cdots \text{Br}_4\text{Q} \cdots \text{I}^-$ unit (Fig. 1) is $-95.36 \text{ kJ mol}^{-1}$ and hence for a single $\text{I}^- \cdots \text{Br}_4\text{Q}$ it is $-46.68 \text{ kJ mol}^{-1}$ or $-11.16 \text{ kcal mol}^{-1}$. This value significantly exceeds our previous estimate of 6–10 kcal mol^{-1} (Molčanov *et al.*, 2018) and is comparable to intermolecular interactions such as hydrogen bonds (Steiner, 2002) and halogen bonds (Stilinović *et al.*, 2017; Eraković *et al.*, 2019). SAPT energy decomposition (Fig. 7) shows that the dominant component of the total interaction is electrostatic ($-86.69 \text{ kJ mol}^{-1}$) followed by dispersion ($-57.09 \text{ kJ mol}^{-1}$).


Figure 5

Symmetry-independent intermolecular critical points in **1**. (3, -1) critical points are shown as red spheres and (3, +1) critical points as blue spheres in the interatomic space; bond paths are shown as red lines.

Table 4

Mulliken and Bader charges calculated in the gas-phase (g) as well as in a periodic system (p).

	Br_4Q (g)		$\text{I}^- \text{Br}_4\text{Q}$ (g)		$\text{I}^- \text{Br}_4\text{Q}$ (p)
	Mulliken	Bader	Mulliken	Bader	Bader
C1	0.239	1.055	0.257	1.022	1.061
O1	-0.223	-1.057	-0.281	-1.048	-1.129
C2	-0.054	-0.049	-0.007	-0.054	-0.096
C3	-0.006	-0.047	0.045	-0.054	-0.094
Br1	0.048	0.048	-0.042	0.019	0.073
Br2	0.050	0.050	-0.049	0.028	0.076
I1			-0.923	-0.765	-0.684
Total Br_4Q	0.000	0.000	-0.077	-0.087	-0.109
Total $\text{I}^- \text{Br}_4\text{Q}$			-1.000	-0.852	-0.793

2.3. Other intermolecular contacts

The AIM (Atoms In Molecule) analysis of intermolecular electron density shows that the highest electron density is found in halogen bonds (Table 3); for C–Br \cdots I it exceeds $0.06 \text{ e}\text{Å}^{-3}$ ($0.09 \text{ e}\text{Å}^{-3}$ in the theoretical model), and it is slightly lower in the C–Cl \cdots I bond. This is in agreement with previous studies, which showed that the strength of halogen bonding involving Br as a donor is comparable to hydrogen bonding (Stilinović *et al.*, 2017) and that it involves a non-negligible covalent component (Eraković *et al.*, 2019). However, despite higher electron density, the C–Br \cdots I halogen bonds are local interactions, whereas the I \cdots quinone interaction is non-localized, dispersed between several centres of the Br_4Q molecule. Therefore, it can be concluded that the halogen bonds are of lesser importance in the crystal packing.

Hydrogen bonding (with the exception of C4–H4 \cdots O1) is weaker, with a maximum electron density below $0.06 \text{ e}\text{Å}^{-3}$ ($0.11 \text{ e}\text{Å}^{-3}$ in the theoretical model, Table 3). Note that two contacts, which satisfy geometric criteria [Table 2 (see also

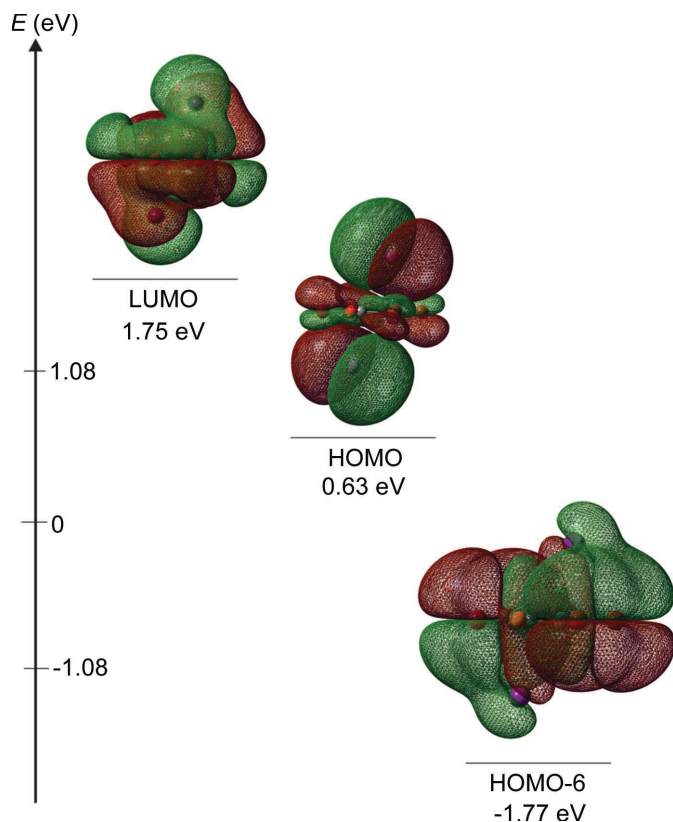


Figure 6
 Calculated HOMOs and LUMOs (at an isovalue of 0.001 e au^{-3}) for the trimer of a tetrabromoquinone molecule and two iodine anions, located at a distance of 3.947 \AA from the centroid of the quinoid ring (as observed in the crystal structure).

Steiner, 2002)] do not have a corresponding $(3, -1)$ critical point, therefore they should not be considered as hydrogen bonds. However, three $\text{C-H}\cdots\text{Br}$ bonds with a $D\cdots A$ distance exceeding 3.9 \AA (Tables 2 and 3) have $(3, -1)$ critical points with electron densities of about 0.03 e \AA^{-3} . This discrepancy between geometric and AIM criteria for weak hydrogen bonding has been noted previously (Milašinić *et al.*, 2020).

3. Conclusions

This work confirmed the nature of the iodide–quinone interaction as a π -hole interaction involving $n \rightarrow \pi^*$ charge transfer. The contact is strongly attractive (its strength and importance in crystal packing are second only to cation–anion electrostatic attraction), with an estimated interaction exceeding $-11 \text{ kcal mol}^{-1}$, and its dominant component is electrostatic with a significant dispersion contribution. However, a relatively low electron density (not exceeding 0.045 e \AA^{-3} , Table 3) found between the iodide and the quinone indicates that the interaction is not localized but dispersed between multiple centres (as shown by the HS and the VDP, Figs. 4 and S10). The estimated degree of charge transfer between the iodide and the quinone is -0.077 to -0.109 e , consistent with the black colour of the crystals.

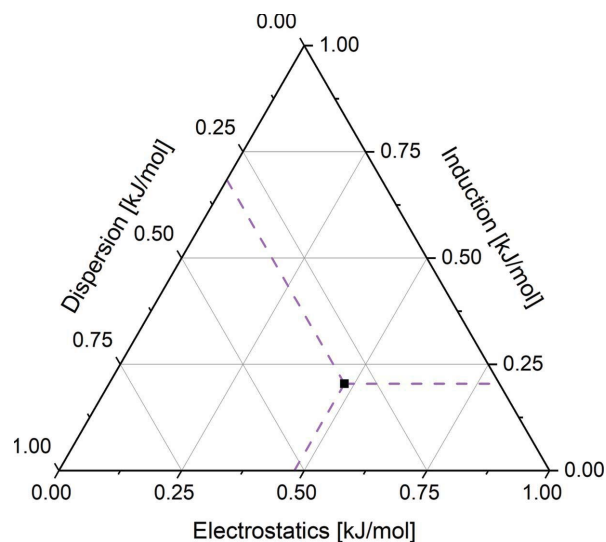


Figure 7
 Ternary plot of the SAPT2+3 decomposition of the interaction energy between the Br_4Q ring and two iodine anions.

Since π -hole interactions between iodide and quinone occur frequently [so far we described more than 20 analogous compounds (Molčanov *et al.*, 2018; Milašinić & Molčanov, 2021)], we expect that they can be employed in crystal engineering. However, since the sandwich-like moiety $\text{I}^- \cdots \text{Br}_4\text{Q} \cdots \text{I}^-$ is probably formed as a stable intermediate in the reduction of the quinone, it can be expected that more electronegative quinones will be reduced to radicals, while the less electronegative ones will not have sufficiently large π -holes. To test the applicability of this interaction in crystal engineering, a larger number of compounds should be tested, including quinones with different substituents (with different electron-withdrawing capabilities) and different nucleophiles (bromine and other halides as well as similar anions such as cyanate, isocyanate, thiocyanate *etc.*).

4. Experimental

4.1. Preparation and basic characterization

All reagents and solvents were purchased from commercial sources (Merck, Sigma–Aldrich, Kemika), were of p.a. purity and were used without further purification.

Compound **1** (Fig. 2) was prepared using an analogous procedure similar to previously studied co-crystals (Molčanov *et al.*, 2018; Milašinić & Molčanov, 2021): an excess of solid 3-chloro-*N*-methylpyridinium iodide was added to a cold (5°C) saturated solution of tetrabromoquinone in acetone. Diffraction-quality single crystals were grown overnight.

4.2. X-ray diffraction and refinement details

Single-crystal XRD data were collected at the Rossendorf Beamline [ESRF, Grenoble, France (Scheinost *et al.*, 2021)] equipped with an Si(111) monochromator and two Pd-coated mirrors. The single-crystal data were recorded with a Pilatus3 X 2M detector (Dectris) with an excitation energy of 20000 eV

per 0.6200926 Å. The monochromator energy was calibrated against the first inflection of the *K*-absorption edge of an Mo metal foil point, tabulated as 20000 eV. The diffraction measurements were performed in shutterless mode with an angular step size of 0.1° and a counting time of 0.1 s per frame. The detector geometry parameters were calibrated with *PyFAI* (Kieffer & Wright, 2013) using a powder pattern of the NIST 660b standard LaB₆. Experimental data were collected using the *Pylatus* software (Dyadkin *et al.*, 2016) and treated using the *SNBL ToolBox* (Dyadkin *et al.*, 2016) and *CrysAlis PRO* (Rigaku OD, 2019).

A total of 131 167 reflections were collected, up to a maximum θ of 40.9° ($d = 0.475$ Å). The multiple integrated reflections were averaged for the space group $P2_1/c$ using *SORTAV* (Blessing, 1987) adapted to the area detector data.

The structure was solved using *SHELXT* (Sheldrick, 2015) and a spherical-atom model was refined using *SHELXL2017* (Sheldrick, 2015). Multipolar refinement was carried out versus all reflections F^2 with the program package *MoPro* (Jelsch *et al.*, 2005). Halogen atoms were modelled as hexadecapoles, O, N and C as octupoles and hydrogens as dipoles; loose restraints were used for multipoles and exponential κ coefficients of chemically equivalent atoms. Vibrations of halogen atoms were refined as anharmonic using fourth-order Gram–Charlier coefficients. Anisotropic parameters for hydrogen atoms were calculated by the *SHADE3* server (Madsen, 2006) and kept fixed in the multipolar atom refinement; aromatic C–H bond lengths were restrained to 1.077 (2) Å and methyl C–H bond lengths to 1.083 (2) Å. Geometry and charge-density calculations and analysis of HSs were performed using *MoPro* (Jelsch *et al.*, 2005); molecular graphics were prepared using *MoProViewer* (Guillot, 2012) and *CCDC-Mercury* (Macrae *et al.*, 2020). Crystallographic and refinement data are shown in Table 5.

Topological bond orders were calculated using the formula (Zarychta *et al.*, 2011)

$$n_{\text{topo}} = a + b\lambda_3 + c(\lambda_1 + \lambda_2) + d\rho_{\text{cp}}.$$

Coefficients a , b , c and d were taken from the literature: for C–C bonds, $a = -0.522$, $b = -1.695$, $c = 0.00$, $d = 8.473$ (Howard & Lamarche, 2003); for C–O bonds, $a = -0.427$, $b = -0.240$, $c = 0.280$, $d = 6.464$ (Tsirelson *et al.*, 2007); for C–N bonds, $a = -0.284$, $b = 0.331$, $c = 0.559$, $d = 6.569$; (Howard & Lamarche, 2003); for C–H bonds $a = -0.153$, $b = 0.481$, $c = 0.983$, $d = 8.087$. (Zhurova *et al.*, 2007).

The analysis of the VDP was achieved using the *Topos PRO* program package (Blatov, 2004).

4.3. Computational details

Gas-phase calculations were carried out in order to obtain more insight into the nature of the quinone–iodide interaction by means of molecular orbitals, atomic charges and interaction energies. Single-point DFT calculations at the B3LYP/def2-SVPD level of theory (Pritchard *et al.*, 2019) were performed using the *GAUSSIAN 16.C.01* program package (Frisch *et al.*, 2016). Grimme D3 dispersion correction (Grimme *et al.*, 2010)

Table 5

Crystallographic data collection and charge-density refinement details.

Compound	1
Empirical formula	C ₁₈ H ₁₄ Br ₄ Cl ₂ I ₂ N ₂ O ₂
Formula weight (g mol ⁻¹)	934.61
Crystal dimensions (mm)	0.12 × 0.09 × 0.09
Space group	$P2_1/c$
a (Å)	6.62900 (10)
b (Å)	11.07760 (10)
c (Å)	17.50330 (10)
α (°)	90
β (°)	97.6870 (10)
γ (°)	90
Z	2
V (Å ³)	1273.776 (14)
D_{calc} (g cm ⁻³)	2.438
μ (mm ⁻¹)	6.226
θ range (°)	1.59–40.93
T (K)	100 (2)
Radiation wavelength	0.62009
Detector type	Dectris Pilatus3 X 2M
Range of h, k, l	$-13 < h < 13$; $-23 < k < 23$; $-36 < l < 36$
Reflections collected	131167
Independent reflections	12766
Reflections with $I \geq 2\sigma$	12766
Absorption correction	Analytical
$T_{\text{min}}, T_{\text{max}}$	0.32961, 1.00000
R_{int}	0.0289
Spherical refinement	
Weighting scheme	$w = 1/[\sigma^2(F_o, 2) + (0.0292P)^2 + 0.2885P]$, where $P = (F_o^2 + 2F_c^2)/3$
R (F)	0.0190
R_w (F^2)	0.0547
Goodness of fit	1.101
Hydrogen atom treatment	Constrained isotropic
No. of parameters	137
No. of restraints	0
$\Delta\rho_{\text{max}}, \Delta\rho_{\text{min}}, \Delta\rho_{\text{r.m.s.}}$ (e Å ⁻³)	1.745; -1.071; 0.115
Multipolar refinement	
Weighting scheme	$w = 1/[6\sigma^2(F_o^2)]$
R (F)	0.0164
R_w (F^2)	0.0403
Goodness of fit	1.125
H atom treatment	Constrained anisotropic
No. of parameters	709
No. of restraints	477
$\Delta\rho_{\text{max}}, \Delta\rho_{\text{min}}, \Delta\rho_{\text{r.m.s.}}$ (e Å ⁻³)	0.488; -0.992; 0.084

was applied in conjunction with the Becke–Johnson damping function and the core electrons for the iodide anions were approximated using pseudopotential functions (Peterson *et al.*, 2003). Bader charges were obtained with the *AIMAll* software (Keith, 2019). The SAPT2+3 level was performed with the *Psi4* software (version 1.3.2; Turney *et al.*, 2012) symmetry-adapted perturbation theory [SAPT (Jeziorski *et al.*, 1994)] using the same basis set as in single-point DFT calculations.

The choice of a smaller def2-SVPD basis set was found to be a good compromise between the efficiency and accuracy of calculations performed. A benchmark study (Parker *et al.*, 2014) found the gold standard of SAPT calculations to be the SAPT2+(3) δ MP2 using the aug-cc-pVTZ basis set. Unfortunately, this basis set, and the other basis sets included in the benchmark study, did not achieve SCF convergence in the single-point calculations when we tried to predict the molecular orbitals with the experimental structure of the chosen fragment, *i.e.* one Br₄Q molecule and two iodine anions.

Moreover, the triple zeta basis sets would have been rather computationally expensive for SAPT calculations beyond SAPT0. Choosing a basis set that is similar to those in the above-mentioned benchmark study, we found that the def2-SVPD did achieve convergence, was small enough to complete SAPT2+3 calculations in a timely fashion and is accurate enough to describe non-covalent interactions correctly, as already discussed in the literature (Witte *et al.*, 2016; 2017). Although we could have extended the single-point calculations that produced the molecular orbital diagrams to a larger def2 basis set, we choose instead to keep the same level of theory for both the molecular orbital calculations and the calculation of the interaction energies. It is also important to point out here that SAPT2+3 calculations are designed to compute energies of dimers. In our studies, we chose a slightly different approach and instead of taking only one iodide anion and quinone ring for consideration, we opted for a trimer, where we treated the Br₄Q molecule as a single unit, and two iodide anions as a second unit. Such a choice was motivated by the specific crystal packing where indeed the interaction between the quinone molecule and two iodide anions occurs simultaneously. Although such an approach is not commonly used, one may find examples in the literature when more than two units were considered (Yourdkhani *et al.*, 2016; Steber *et al.*, 2017).

To further support the discussion on the nature of intra- and intermolecular interactions in the crystalline state, periodic DFT was engaged with the use of the *CRYSTAL17* software (Dovesi *et al.*, 2018). Calculations were performed on the PBE0/POB-DZVP level of theory (Vilela Oliveira *et al.*, 2019) applying an additional Grimme's D3 correction (Grimme *et al.*, 2010). Atomic coordinates were taken from the X-ray diffraction experiment and were kept frozen during modelling. Periodic wavefunctions obtained in such a way were further used to carry out the topological analysis of periodic electron densities. The QTAIM approach was adopted (Bader, 1990) using the *TOPOND14* program (Gatti & Casassa, 2017) integrated with *CRYSTAL17*.

Funding information

Financial support by the Croatian Science Foundation (grant no. IP-2019-04-4674) is gratefully acknowledged. This research was supported in part by PL-Grid Infrastructure (grant no. plgrhopolar1e).

References

- Angarov, V. & Kozuch, S. (2018). *New J. Chem.* **42**, 1413–1422.
- Bader, R. F. W. (1990). *Atoms in Molecules – A Quantum Theory*. Oxford University Press.
- Bauzá, A., Mooibroek, T. J. & Frontera, A. (2016). *CrystEngComm*, **18**, 10–23.
- Bauzá, A., Seth, S. K. & Frontera, A. (2019). *Coord. Chem. Rev.* **384**, 107–125.
- Blatov, V. A. (2004). *Crystallogr. Rev.* **10**, 249–318.
- Blessing, R. H. (1987). *Crystallogr. Rev.* **1**, 3–58.
- Dovesi, R., Erba, A., Orlando, R., Zicovich-Wilson, C. M., Civalleri, B., Maschio, L., Rérat, M., Casassa, S., Baima, J., Salustro, S. & Kirtman, B. (2018). *WIREs Comput. Mol. Sci.* **8**, e1360.
- Dyadkin, V., Pattison, P., Dmitriev, V. & Chernyshov, D. (2016). *J. Synchrotron Rad.* **23**, 825–829.
- Eraković, M., Cinić, D., Molčanov, K. & Stilinović, V. (2019). *Angew. Chem. Int. Ed.* **58**, 15702–15706.
- Frisch, M. J., Trucks, G. W., Schlegel, H. B., Scuseria, G. E., Robb, M. A., Cheeseman, J. R., Scalmani, G., Barone, V., Petersson, G. A., Nakatsuji, H., Li, X., Caricato, M., Marenich, A. V., Bloino, J., Janesko, B. G., Gomperts, R., Mennucci, B., Hratchian, H. P., Ortiz, J. V., Izmaylov, A. F., Sonnenberg, J. L., Williams-Young, D., Ding, F., Lipparini, F., Egidi, F., Goings, J., Peng, B., Petrone, A., Henderson, T., Ranasinghe, D., Zakrzewski, V. G., Gao, J., Rega, N., Zheng, G., Liang, W., Hada, M., Ehara, M., Toyota, K., Fukuda, R., Hasegawa, J., Ishida, M., Nakajima, T., Honda, Y., Kitao, O., Nakai, H., Vreven, T., Throssell, K., Montgomery, J. A. Jr, Peralta, J. E., Ogliaro, F., Bearpark, M. J., Heyd, J. J., Brothers, E. N., Kudin, K. N., Staroverov, V. N., Keith, T. A., Kobayashi, R., Normand, J., Raghavachari, K., Rendell, A. P., Burant, J. C., Iyengar, S. S., Tomasi, J., Cossi, M., Millam, J. M., Klene, M., Adamo, C., Cammi, R., Ochterski, J. W., Martin, R. L., Morokuma, K., Farkas, O., Foresman, J. B. & Fox, D. J. (2016). *Gaussian 16, Revision C. 01* Gaussian, Inc., Wallingford CT, USA.
- Frontera, A., Gamez, P., Mascal, M., Mooibroek, T. J. & Reedijk, J. (2011). *Angew. Chem. Int. Ed.* **50**, 9564–9583.
- Gamez, P., Mooibroek, T. J., Teat, S. J. & Reedijk, J. (2007). *Acc. Chem. Res.* **40**, 435–444.
- Gatti, C. & Casassa, S. (2017). *TOPOND14* User's Manual. CNR-ISTM, Milan, Italy.
- Grimme, S., Antony, J., Ehrlich, S. & Krieg, H. (2010). *J. Chem. Phys.* **132**, 154104–19.
- Grounds, O., Zeller, M. & Rosokha, S. V. (2018). *New J. Chem.* **42**, 10572–10583.
- Guillot, B. (2012). *Acta Cryst.* **A68**, s204.
- Howard, S. T. & Lamarche, O. (2003). *J. Phys. Org. Chem.* **16**, 133–141.
- Jelsch, C., Guillot, B., Lagoutte, A. & Lecomte, C. (2005). *J. Appl. Cryst.* **38**, 38–54.
- Jeziorski, B., Moszynski, R. & Szalewicz, K. (1994). *Chem. Rev.* **94**, 1887–1930.
- Jia, C., Miao, H. & Hay, B. P. (2019). *Cryst. Growth Des.* **19**, 6806–6821.
- Keith, T. A. (2019). *AIMAll*. TK Gristmill Software, Overland Park, KS, USA.
- Kepler, S., Zeller, M. & Rosokha, S. V. (2019). *J. Am. Chem. Soc.* **141**, 9338–9348.
- Kieffer, J. & Wright, J. P. (2013). *Powder Diffr.* **28**, 339–350.
- Kozuch, S. (2016). *Phys. Chem. Chem. Phys.* **18**, 30366–30369.
- Kumar Seth, S., Bauzá, A. & Frontera, A. (2019). *Quantitative Analysis of Weak Non-covalent s-Hole and p-Hole Interactions*, in D. Chopra (ed.) *Understanding Intermolecular Interactions in the Solid State: Approaches and Techniques*. London: Royal Society of Chemistry.
- Lucas, X., Bauzá, A., Frontera, A. & Quiñero, D. (2016). *Chem. Sci.* **7**, 1038–1050.
- Macrae, C. F., Sovago, I., Cottrell, S. J., Galek, P. T. A., McCabe, P., Pidcock, E., Platings, M., Shields, G. P., Stevens, J. S., Towler, M. & Wood, P. A. (2020). *J. Appl. Cryst.* **53**, 226–235.
- Madsen, A. Ø. (2006). *J. Appl. Cryst.* **39**, 757–758.
- Milašinović, V., Krawczuk, A., Molčanov, K. & Kojić-Prodić, B. (2020). *Cryst. Growth Des.* **20**, 5435–5443.
- Milašinović, V. & Molčanov, K. (2021). *CrystEngComm*, **23**, 8209–8214.
- Molčanov, K., Jelsch, C., Landeros, B., Hernández-Trujillo, J., Wenger, E., Stilinović, V., Kojić-Prodić, B. & Escudero-Adán, E. C. (2019). *Cryst. Growth Des.* **19**, 391–402.
- Molčanov, K., Mali, G., Grdadolnik, J., Stare, J., Stilinović, V. & Kojić-Prodić, B. (2018). *Cryst. Growth Des.* **18**, 5182–5193.
- Mooibroek, T. J., Gamez, P. & Reedijk, J. (2008). *CrystEngComm*, **10**, 1501–1515.

- Newberry, R. W. & Raines, R. T. (2017). *Acc. Chem. Res.* **50**, 1838–1846.
- Parker, T. M., Burns, L. A., Parrish, R. M., Ryno, A. G. & Sherrill, C. D. (2014). *J. Chem. Phys.* **140**, 094106–16.
- Peterson, K. A., Figgen, D., Goll, E., Stoll, H. & Dolg, M. (2003). *J. Chem. Phys.* **119**, 11113–11123.
- Pritchard, B. P., Altarawy, D., Didier, B., Gibson, T. D. & Windus, T. L. (2019). *J. Chem. Inf. Model.* **59**, 4814–4820.
- Rigaku OD (2019). *Crysalis PRO* Rigaku Oxford Diffraction Ltd, Yarnton, Oxfordshire, England.
- Savastano, M., Bazzicalupi, C., García, C., Gellini, C., López de la Torre, M. D., Mariani, P., Pichierri, F., Bianchi, A. & Melguizo, M. (2017). *Dalton Trans.* **46**, 4518–4529.
- Scheinost, A. C., Claussner, J., Exner, J., Feig, M., Findeisen, S., Hennig, C., Kvashnina, K. O., Naudet, D., Prieur, D., Rossberg, A., Schmidt, M., Qiu, C., Colomp, P., Cohen, C., Dettona, E., Dyadkin, V. & Stumpf, T. (2021). *J. Synchrotron Rad.* **28**, 333–349.
- Schottel, B. L., Chifotides, H. T. & Dunbar, K. R. (2008). *Chem. Soc. Rev.* **37**, 68–83.
- Seth, S. K., Bauzá, A., Mahmoudi, G., Stilinović, V., López-Torres, E., Zaragoza, G., Keramidas, A. D. & Frontera, A. (2018). *CrystEngComm*, **20**, 5033–5044.
- Sheldrick, G. M. (2015). *Acta Cryst.* **A71**, 3–8.
- Sheldrick, G. M. (2015). *Acta Cryst.* **C71**, 3–8.
- Singh, S. K. & Das, A. (2015). *Phys. Chem. Chem. Phys.* **17**, 9596–9612.
- Spackman, P. R., Turner, M. J., McKinnon, J. J., Wolff, S. K., Grimwood, D. J., Jayatilaka, D. & Spackman, M. A. (2021). *J. Appl. Cryst.* **54**, 1006–1011.
- Steber, A. L., Pérez, C., Temelso, B., Shields, G. C., Rijs, A. M., Pate, B. H., Kisiel, Z. & Schnell, M. (2017). *J. Phys. Chem. Lett.* **8**, 5744–5750.
- Steiner, T. (2002). *Angew. Chem. Int. Ed.* **41**, 48–76.
- Stilinović, V., Horvat, G., Hrenar, T., Nemeč, V. & Cinčić, D. (2017). *Chem. Eur. J.* **23**, 5244–5257.
- Tsirelson, V. G., Bartashevich, E. V., Stash, A. I. & Potemkin, V. A. (2007). *J. Am. Chem. Soc.* **129**, 13887–13893.
- Turney, J. M., Simmonett, A. C., Parrish, R. M., Hohenstein, E. G., Evangelista, F., Fermann, J. T., Mintz, B. J., Burns, L. A., Wilke, J. J., Abrams, M. L., Russ, N. J., Leininger, M. L., Janssen, C. L., Seidl, E. T., Allen, W. D., Schaefer, H. F., King, R. A., Valeev, E. F., Sherrill, C. D. & Crawford, T. D. (2012). *WIREs Comput. Mol. Sci.* **2**, 556–565.
- Vilela Oliveira, D., Laun, J., Peintinger, M. F. & Bredow, T. (2019). *J. Comput. Chem.* **40**, 2364–2376.
- Vuković, V., Molčanov, K., Jelsch, C., Wenger, E., Krawczuk, A., Jurić, M., Androš Dubraja, L. & Kojić-Prodić, B. (2019). *Cryst. Growth Des.* **19**, 2802–2810.
- Wang, D.-X. & Wang, M.-X. (2013). *J. Am. Chem. Soc.* **135**, 892–897.
- Wilson, J., Maxson, T., Wright, I., Zeller, M. & Rosokha, S. V. (2020). *Dalton Trans.* **49**, 8734–8743.
- Witte, J., Neaton, J. B. & Head-Gordon, M. (2016). *J. Chem. Phys.* **144**, 194306–12.
- Witte, J., Neaton, J. B. & Head-Gordon, M. (2017). *J. Chem. Phys.* **146**, 234105–10.
- Yourdkhani, S., Chojecki, M., Hapka, M. & Korona, T. (2016). *J. Phys. Chem. A*, **120**, 6287–6302.
- Zarychta, B., Zaleski, J., Kyzioł, J., Daszkiewicz, Z. & Jelsch, C. (2011). *Acta Cryst.* **B67**, 250–262.
- Zeng, H., Liu, P., Feng, G. & Huang, F. (2019). *J. Am. Chem. Soc.* **141**, 16501–16511.
- Zhurova, E. A., Zhurov, V. V. & Pinkerton, A. A. (2007). *J. Am. Chem. Soc.* **129**, 13887–13893.